Title
Limit Cycle and Anomalous Capacitance in the Kondo Insulator SmB6

Journal
Physical Review Letters, 109(9)

ISSN
0031-9007

Authors
Kim, DJ
Grant, T
Fisk, Z

Publication Date
2012-08-31

DOI
10.1103/physrevlett.109.096601

Limit Cycle and Anomalous Capacitance in the Kondo Insulator SmB_6

D. J. Kim, T. Grant, and Z. Fisk

Department of Physics and Astronomy, University of California, Irvine, California 92697, USA

(Received 19 April 2012; published 29 August 2012)

We report a frequency coding limit cycle and anomalous capacitance in the Kondo insulator SmB_6 at low temperatures where the insulating gap becomes fully opened. The limit cycle appears to be associated with local activity and autocatalytic temporal pattern formation, as occurs in biological systems. The measured anomalous capacitance may indicate surface and bulk separation, suggesting the formation of a surface conducting state. The biological analogy suggests lossless information transport and complex information coding, and the surface state with a superconductor would provide a possible venue for quantum computing resources without decoherence.

DOI: 10.1103/PhysRevLett.109.096601 PACS numbers: 72.15.Qm, 71.20.Eh, 72.20.Ht

With the shrinking of integrated electronic devices, quantum phenomena can lead to device malfunction and unreliability [1,2]. While enormous effort has been made to avoid these side effects [3], they suggest investigating new possibilities in nanodevices exhibiting single electron physics [4], spin transport [5,6], and qubits for quantum computation [7,8] with much higher computational power from its intrinsic parallelism. Biological parallel computation exists inside the human brain and is based on neurons [9]. Artificial neural networks provide another approach to realize parallelism [10–12]. Even though the biological brain contains an extremely complex network of neurons with very diverse structures, the neurons, the basic unit of computation, share certain structural and functional similarities [13]. Thus, functional materials mimicking the functions of a biological neuron are critical for the implementation of parallelism with nonbiological components.

Kondo insulators [14] are highly correlated electron materials that develop a narrow gap through hybridization effects, as seen, for example, in electrical resistivity increasing steeply at low temperatures. Single crystals of the Kondo insulator of SmB_6 have a 4–5 order increase of resistance at low temperatures due to this indirect gap from hybridization between f and conduction bands, as shown in Fig. 1. At 2 K, the material can be driven into a dissipative regime with increasing current, and the current to voltage (I-V) relation shows nonlinear negative differential resistance (NDR) from self heating (upper right inset of Fig. 1). The development of the NDR curves that start from different base temperatures is not, however, just due to a static resistance drop from sample heating, but possesses intrinsic nonlinear dynamic characteristics. Electron temperature has its own complex dynamics in the nonlinear regime, and correspondingly the voltage and current have a complex relation with nonlinear resistance R and dependence on electron temperature T_e, which we write as

$$V_s = R_s(T_e, I)I_s. \quad (1)$$

Like transition metal oxides, which undergo a metal insulator transition, the electrical contact resistance to Kondo insulators is proportional to the temperature-dependent sample resistance and increases at low temperatures. Four probe measurements were used for all measurements, except the oscillation on SmB_6 to avoid contact effects. To minimize the local contact heating and impedance load effect in the current leads, we used several *Pt* wires and many point spot welding for leads, and this dramatically reduced the total contact resistance and provided uniform current flow on the sample surface. The cryostat base thermometer cannot properly read temperature changes from local joule heating of the SmB_6 as the bias current flows, so we employed a surface-mounted Cernox thermometer on top of the sample to read temperature changes. At the interface between the Cernox thermometer and the wired SmB_6 surface, a thin N greased

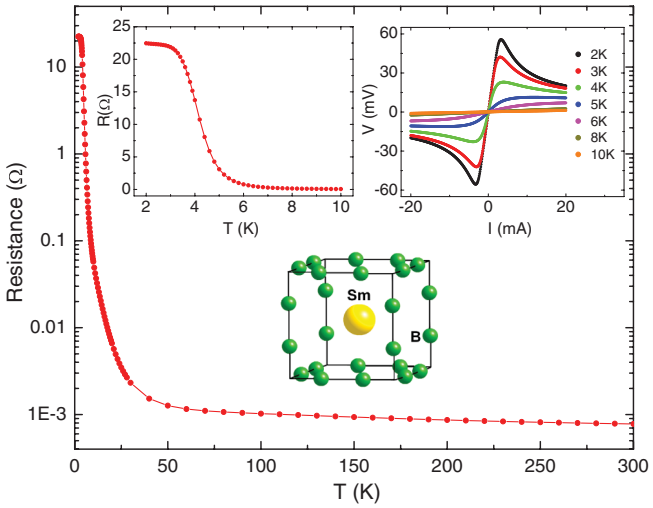

FIG. 1 (color). Temperature dependency of resistance of SmB_6 single crystal. The left inset shows a low temperature resistance versus temperature plot, and the right inset shows current versus voltage plots at various temperatures. The lower inset shows the crystal structure of SmB_6.

cigarette paper was placed to ensure thermal anchoring and electrical insulation. In this way, we could confirm that the sample temperature is increased by joule heating. We used both Keithely 2612A SMU and home-made low-noise electronics together with a PAR 5301 lock-in amplifier for small-signal ac measurements. The real-time Lissajous curves were measured using an NI 6259 DAQ board, a bipolar current source, and a synchronous data acquisition and generation program.

As depicted in Fig. 2(a), the axon in the nerve system, corresponding to an information transmission line, has two important properties. One is the active or lossless propagation of a nerve impulse, and the other is the frequency coding with which information is encoded in the frequency of the action potential with changing amplitude of the stimulus voltage [9,13]; a neuron works as a voltage-to-frequency converter. For SmB_6, a setup depicted in Fig. 2(d) is used to drive oscillations with a dc current source, and Fig. 2(b) shows that the frequency of the oscillation has a clear dependence on stimulus current, working as a current-to-frequency converter.

Macroscopically, an oscillation arises from loss of linear stability. Instead of going to a thermal and electrical equilibrium state with irreversible heat exchange, beyond a threshold current the instability drives a limit cycle. Oscillation occurs only with at least 50 μF capacitance

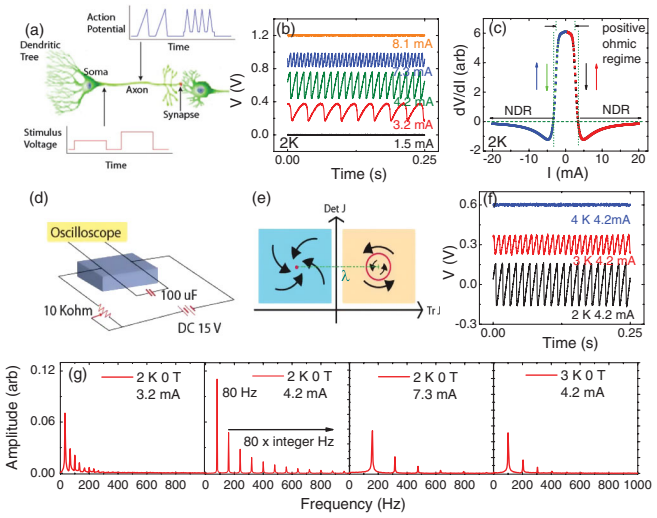

FIG. 2 (color). Self-sustained oscillation of SmB_6. (a) Frequency coding of action potential in nerve system. Information is encoded in the frequency change with stimulus voltage. (b) Frequency coding by stimulus current in SmB_6 after insulating gap is developed; curves have been offset for clarity. (c) dV/dI plot at 2 K. In Fig. 2(b), the oscillation is confined to the NDR regime. (d) The measurement setup. (e) The oscillation is due to bifurcation from a stable focus to a limit cycle, the polarity change of λ originates at the minimum capacitance necessary to trigger the oscillation. (f) Temperature dependence of oscillation; curves have been offset for clarity (g) Fast Fourier transforms of the oscillations.

across the SmB_6 sample in the setup of Fig. 2(d). This marginal value of capacitance indicates that the instability is a transition from a stable focus to a limit cycle beyond the threshold current. A simple analysis of the circuit in Fig. 2(d) leads to a differential equation for the circuit in the form $dV_s(t)/dt = -I_s(T_s, V_s)/C - (V_s - V)/RC$. Considering the electron temperature as an internal degree of freedom, its dynamics can be expressed as $dTe/dt = A(Te, Vs)$. These two autocatalytic reactions have a corresponding Jacobian matrix for instability analysis [15].

$$J = \begin{vmatrix} \frac{\partial A(T_e,V_s)}{\partial T_e} & \frac{\partial A(T_e,V_s)}{\partial V_s} \\ \frac{1}{C}\frac{\partial I_s(T_e,V_s)}{\partial T_e} & \frac{1}{C}\left(\frac{1}{R} + \frac{\partial I_s(T_e,V_s)}{\partial V_s}\right) \end{vmatrix}. \quad (2)$$

This matrix has two complex conjugate eigenvalues $\lambda \pm i\omega$ (λ, ω real), and as shown in Fig. 2(e), the Hopf bifurcation from a stable point to a limit cycle occurs when the eigenvalues cross the imaginary axis with NDR; thus, Det $J > 0$ and Tr $J > 0$. These two conditions are equivalent to the NDR and a critical value of capacitance C_0. Thus, as the total capacitance exceeds the critical value of C_0, the trace of the Jacobian matrix becomes positive, leading the system to self-sustained oscillation with approximate time scale τ.

$$C_0 = \left(\frac{\partial I_e}{\partial V_s} + \frac{1}{R}\right)\left(\frac{\partial A}{\partial T_e}\right)^{-1}, \qquad \tau \sim \left(\frac{1}{C}\left(\frac{1}{R} + \frac{\partial I_s}{\partial V_s}\right)\right)^{-1}. \quad (3)$$

A threshold and a maximum value exist between which the limit cycle activity appears, where both the frequency and amplitude of the oscillation have monotonic dependence on the dc current. Over the entire range where oscillations occur, there are only stable frequencies and their subharmonics [Fig. 2(g)]. Even though the NDR persists clearly in I-V and dV/dI curves above the platform temperature of 5 K, the oscillation immediately disappears as the platform temperature goes over 4 K. This onset temperature was independent of the sample measured and contact resistances, and corresponds to the temperature below which the resistance value saturates, which we interpret as the complete opening of the indirect gap of SmB_6. The resistance R is used to control the current flowing through SmB_6 and is inversely proportional to the current; thus, the frequency $1/\tau$ is proportional to the current impulse, simply mimicking frequency coding in a nerve neuron where the amplitude of stimulus is converted into the frequency of the nerve impulse. This may provide a more complex artificial neuron than the binary McCulloch-Pitts model [16].

The above argument confirms the NDR of SmB_6 and its intrinsic local activity. All electrical transmission lines have loss, but in the nerve axon the all-or-none property of action potential makes it possible to propagate information without attenuation. In solid-state electronics, this lossless information transport can be realized by positioning this local active device along signal lines and providing energy or amplification to the successive section of line, as

in Crane's neuristor [17]. This is important for the scalability of artificial solid-state neural systems to overcome the intrinsic limit of signal loss.

The slow response of the SmB_6 oscillator can be explained by its similarity to the Hodgkin-Huxley model, in which the electrical properties between the endocell and exocell are described by the membrane capacitance and the time-varying nonlinear ion channel conductance. This similarity is shown in Fig. 3. We used a hardware-timed synchronous data generation and acquisition setup to acquire the whole history of Lissajous curves from the very beginning of the current excitation. Figure 3 clearly shows time evolution of the Lissajous curves with driving frequency at base temperature of 2 K. In Fig. 3(a), with a low driving frequency of 1 Hz, self heating and cooling through the lattice are balanced and all Lissajous curves overlap, and there is no time evolution in the I-V relation, just very clear hysteresis. As the frequency increases [see Figs. 3(b)–3(h)], the Lissajous curves have clear time dependence and

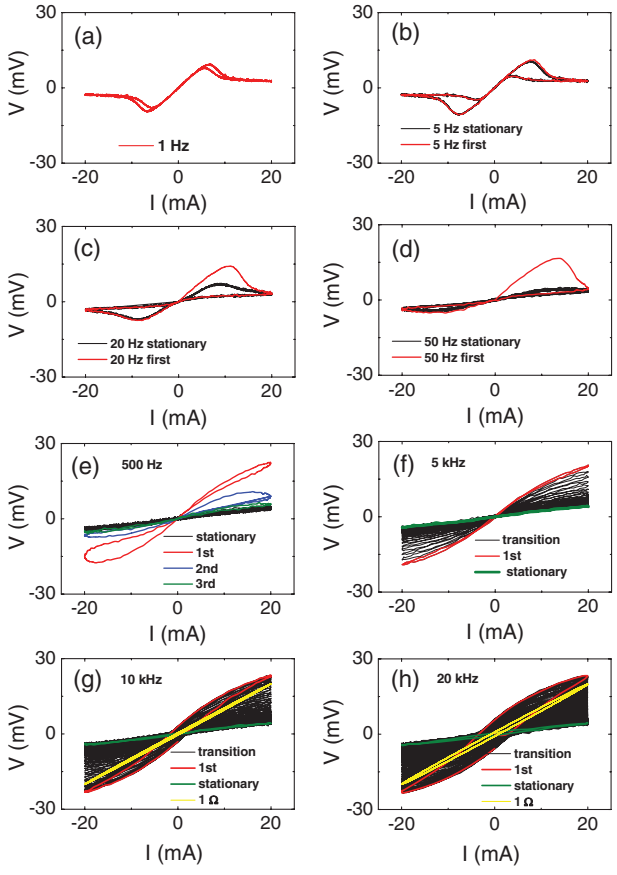

FIG. 3 (color). Frequency dependence of Lissajous plots. (a) 1 Hz plot where continued cycling overlaps the initial trace and shows hysteresis from virtual thermal impedance. (b)–(e) Evolution of hysteresis plots with temperature and eventual saturation at final state. (f)–(h) The final states have the same resistive impedance. Above 10 kHz, hysteresis becomes conspicuous in Ohmic regime, the yellow lines showing Lissajous curves for the 1 Ω resistor at 10 and 20 kHz.

differing initial and final impedance states. As the frequency increases, the final state resistance becomes smaller and almost saturates from 500 Hz to 20 kHz. In high-frequency plots above 10 kHz, hysteresis appears even in the Ohmic regime. The pinched hysteresis loops in Figs. 3(a)–3(e) with low frequencies reflect the development of virtual thermal impedance [18]. The energy balance can be described by generated energy (ΔP) = stored energy ($Cd(\Delta T)/dt$) + dissipative energy ($D\Delta T$), where ΔT is the temperature variation corresponding to power variation ΔP, C the specific heat, and D the dissipation constant. With the temperature coefficient given by $\alpha = \Delta R/(R\Delta T)$, the above energy relation leads to the general form of frequency dependence impedance for sinusoidal perturbation as

$$R = 1/\left(\frac{D - \alpha P}{2\alpha PR}\right) + i\omega\left(\frac{C}{2\alpha PR}\right). \quad (4)$$

The above impedance converges to simple resistance R when there is negligible power generation from self heating, and has meaning only when it goes beyond the Ohmic regime. At zero frequency, the virtual capacitance term has no meaning, and hystereses in the first and third quadrants disappear; in contrast, the increasing frequency leads to hysteresis, a phase shift in small signal ac I-V relation, and also removes the NDR effect in dV/dI curves.

Very unusual behavior is observed with low-resistance samples in high-frequency Lissajous plots. Above 5 kHz, the Lissajous curve starts to show hysteresis even in the Ohmic regime [see Figs. 3(g) and 3(h)] with the same final state. The final state does not have any frequency dependence, suggesting that its impedance is very resistive. This implies that SmB_6 is not in the class of Chua's memristor [18,19]. The sample used in Figs. 3 and 4 has only 1.8 Ω (contact resistance of 3 Ω for each contact), and this low resistance and Ohmic contacts are important to discriminate clearly the origin of the hysteresis from the thermal and contact effects. The yellow lines in Figs. 3(g) and 3(h) show the Lissajous curve of 1 Ω resistor at 10 and 20 kHz for 20 mA peak ac current exhibiting a reasonably linear relation, with a slight time lag coming from the measurement electronics and wires in the cryostat. Upon replacing the 1 Ω resistor with a 1.8 Ω SmB_6 single crystal, we see a remarkable time lag equivalent to an 800 nF capacitance across the SmB_6 [20–22]. This is an unusually large value of capacitance, which cannot be explained as a simple resistive material and its Ohmic contacts.

This unusual onset of capacitance in SmB_6 is confirmed by the time evolution of the Lissajous curve shown in Figs. 4(a)–4(f) measured at 2 K base temperature. Initially, the curve is metastable at a short period (500 μs), and then starts the thermal evolution to the final state. During the evolution, the RC time constant becomes small, and eventually the delay between the current and voltage becomes negligible in the final state. As shown in

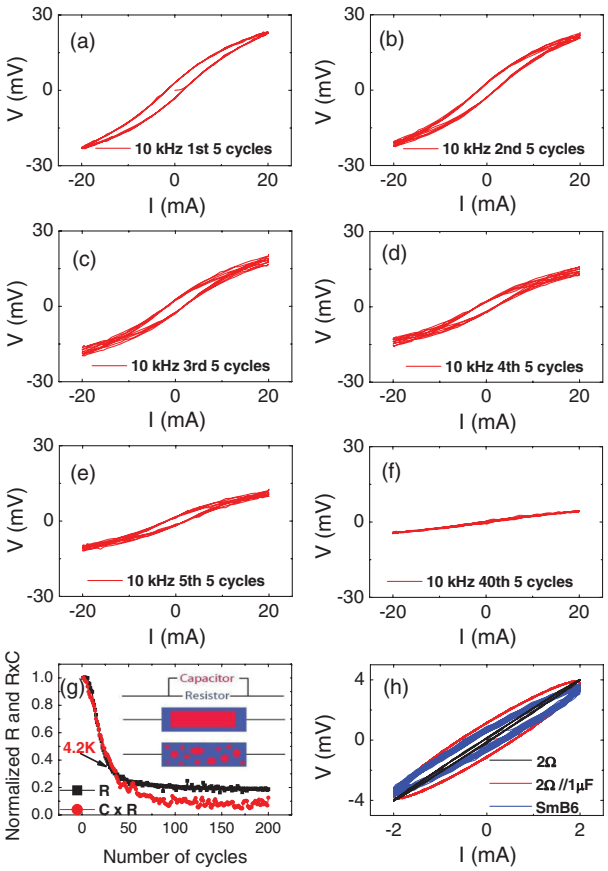

FIG. 4 (color). Time evolution of 10 kHz Lissajous plots. (a): the first five cycles are in a metastable state. (b)–(f): the resistance drop and the zero point hysteresis pinching by heating. (g): The resistance and time constant drop with the number of cycles due to heating. Above 4.2 K sample temperature, the capacitance disappears, the inset showing the topologically equivalent *RC* circuit with possible *RC* contributions, blue representing conducting layer and red high dielectric insulating regimes. (h): low current Lissajous plot in Ohmic regime.

Fig. 4(g), the time constant drop becomes faster than the resistance drop after 4.2 K. This may indicate that the onset of the capacitance has temperature dependence, and capacitance has a constant value only below the temperature where the indirect gap is completely formed. We were able to confirm that even the high-resistance sample used in Figs. 1 and 2, which changes from 23 Ω (2 K) to 1.4 Ω (6 K) by heating, shows no hysteresis in the Ohmic regime of the final 6 K state [23]. Thus, the disappearance of the hysteresis is caused by the resistance drop, and it reflects the dramatic change of capacitance with temperature, leading the hysteresis to become smaller at higher temperatures. Figure 4(h) shows the Lissajous plots of low current (2 mA) 20 kHz excitation for 2 Ω, 2 Ω parallel to 1 μF, and 1.8 Ω SmB_6 samples. Unlike the pure 2 Ω resistor, SmB_6 is close to the plot of 2 Ω parallel to 1 μF. Thus, it is natural to think of SmB_6 modeled as an *RC* circuit, which suggests that the origin of the capacitance might possibly be from a real transition inside the material. An *RC* circuit is topologically equivalent to an insulating material encapsulated with a conducting surface in a bulk material. There are two possibilities, one is a uniform insulating bulk encapsulated by a conducting layer, and the other is many insulating grains embedded in a conducting bulk, as depicted in the inset of Fig. 4(g). The uniformity and huge capacitance suggest that the first model is more reasonable since, as SmB_6 opens its insulating gap completely at low temperatures, the bulk becomes an insulator with high dielectric constant making an equivalent *RC* circuit, which can be used to explain the observed phenomena. The Kondo insulator SmB_6 appears to have an intrinsic metal to high dielectric transition at low temperatures, leading to an intrinsic parallel *RC* circuit and a topological surface state [24].

In summary, we observed a limit cycle and anomalous capacitance formation in SmB_6 single crystals at low temperatures where the insulating gap is fully opened. Thermally driven dynamical instability causes self-sustained oscillation, and the frequency dependence with driving current mimics the electrical properties of a biological neural system. The huge capacitance formation in small-size crystals at low temperatures indicates that the bulk has very high dielectric constants and heterogeneous electrical properties arising from the surface that is still highly conductive. The surface state with high dielectric bulk suggests various experiments, including insulated surface gate structure, imaging of surface state, and precise surface spectroscopy. Proximity effects might reveal new electrical properties for exploring quantum computational resource without quantum phase decoherence.

The authors thank L. Chua, J. Flouquet, Y. Haga, S. Brown, X. Lu, P. Pagliuso, and I. K. Schuller for discussions. This research was supported by NSF-DMR-0801253.

[1] J. D. Meindl, Q. Chen, and J. A. Davis, Science **293**, 2044 (2001).
[2] R. W. Keyes, Proc. IEEE **89**, 227 (2001).
[3] S. E. Thompson *et al.*, Mater. Today **9**, 20 (2006).
[4] M. A. Kastner, Rev. Mod. Phys. **64**, 849 (1992).
[5] I. Zutic *et al.*, Rev. Mod. Phys. **76**, 323 (2004).
[6] S. A. Wolf *et al.*, Science **294**, 1488 (2001).
[7] A. Steane, Rep. Prog. Phys. **61**, 117 (1998).
[8] C. Nayak, Rev. Mod. Phys. **80**, 1083 (2008).
[9] C. F. Steven, *Neurophysiology: A Primer* (Wiley, New York, 1966).
[10] L. S. Smith, *Handbook of Nature-Inspired and Innovative Computing: Integrating Classical Models with Emerging Technologies* (Springer, New York, 2006).
[11] M. Tsodyks and C. Gilbert, Nature (London) **431**, 775 (2004).
[12] H. Markram, Neuroscience (N.Y.) **7**, 153 (2006).
[13] J. Nolte, *The Human Brain : An introduction to Its Functional Anatomy* (Mosby, St. Louis, MO, 2002).
[14] G. Aeppli and Z. Fisk, Comments Condens. Matter Phys. **16**, 155 (1992).

[15] E. Scholl, *Nonlinear Spatio-Temporal Dynamics and Chaos in Semiconductor* (Cambridge University Press, Cambridge, England, 2001).
[16] W. McCulloch and W. Pitts, Bull. Math. Biol. **7**, 115 (1943).
[17] H. D. Crane, Proc. IRE **50**, 2048 (1962).
[18] D. J. Kim and Z. Fisk, Appl. Phys. Lett. **101**, 013505 (2012).
[19] L. Chua, Appl. Phys. A **102**, 765 (2011).
[20] P. Simon and Y. Gogotsi, Nature Mater. **7**, 845 (2008).
[21] B. Skinner, M. S. Loth, and B. I. Shklovskii, Phys. Rev. Lett. **104**, 128302 (2010).
[22] A. L. Efros, Phys. Rev. B **84**, 155134 (2011).
[23] See Supplemental Material at http://link.aps.org/supplemental/10.1103/PhysRevLett.109.096601 for details.
[24] M. Dzero, K. Sun, V. Galitski, and P. Coleman, Phys. Rev. Lett. **104**, 106408 (2010).